CFD simulation and second law analysis of weir-type cascade solar stills with different number and dimensions of steps

Fatemeh Alipanah[a], Nader Rahbar[b,c]*

[a]*Department of Mechanical Engineering, Semnan Branch, Islamic Azad University, P.O. Box 35196-97951, Semnan, Iran, Tel. +98-231-3354040; Fax: +98-231-3354030; email: fateme.alipanah@gmail.com*
[b]*Young Researchers and Elite Clubs, Semnan Branch, Islamic Azad University, Semnan, Iran*
[c]*Energy and Sustainable Development Research Center, Semnan Branch, Islamic Azad University, P.O. Box 35196-97951, Semnan, Iran, Tel. +98-231-3354040; Fax: +98-231-3354030; emails: nrahbar@gmail.com, rahbar@semnaniau.ac.ir (N. Rahbar)*

ABSTRACT

Computational fluid dynamics (CFD) simulation of fluid flow in weir-type cascade solar stills with different geometries has been presented in this paper. The results of CFD simulation were also used to estimate local entropy generation inside the weir-type solar stills. The results showed that maximum water production was achieved with 7, 8 and 10 steps when the step height was 2 cm. In addition, considering number of steps and various steps heights, the case with six steps of 3.5 cm height was found to be the best geometry for the investigated solar still. Moreover, the results of the simulation show that the number of recirculating zones and their regularity are the main parameters affecting the productivity of a weir-type cascade solar still. Contours of isotherms, vapor mass fraction, streamlines and local entropy generation have been presented in order to demonstrate their contribution to the behavior of the investigated solar still. Furthermore, the results of second law analysis showed that the most entropy generation occurred near the glass and the water surface, as well as at the tip of the stairs. This entropy generation was mainly due to the heat and mass transfer phenomena and the fluid friction.

Keywords: CFD simulation; Weir-type cascade solar still; Double diffusive natural convection; Heat and mass transfer; Entropy generation; Second law analysis

1. Introduction

Fresh air and clear water are two vital components of life. In many arid regions of the world including coastal, remote and dry areas there is no sufficient resources for producing electrical power to desalinate water. Therefore, over such regions, there is a need to seek appropriate techniques and technologies to make potable water.

Water desalination methods, such as distillation, reverse osmosis or electrodialysis, are generally based on thermal and membrane approaches. An appropriate desalination method should provide features such as low and clean energy consumption, high quality, good efficiency, ease of usage and low cost. Hence, distillation could be seen as a preferred method of water desalination. Solar water desalination systems can be a good choice to desalinate salt water within regions of high solar irradiation. Many empirical studies and theoretical analysis used to investigate performance and factors contributing to the efficiency of solar desalination systems [1–8].

Theoretical analysis can be also classified into two categories of mathematical modeling and numerical simulation. The significant advantage of numerical simulation or computational fluid dynamics (CFD) over their counterparts is based on the fact that fluid velocity, pressure and flow patterns can be easily observed by such methodologies. Furthermore, factors affecting the performance, either beneficial or harmful, can be easily recognized, so that attempts can be made to either solve the latter or improve the former. On the other hand, due to simple adjustability of parameters, such as geometric dimensions and boundary conditions, numerical analysis is an effective method that can help in the performance

---

* Corresponding author.

study of energy systems through changing various parameters. However, numerical simulation has the following limitations and a designer should be aware of these limitations when using the CFD methods. However, numerical simulation has the following limitations and a designer should be aware of these limitations when using the CFD methods [9–14]:

- Establishing the solving algorithm is difficult on some CFD codes.
- Convergence of solutions is time consuming in some CFD algorithms.
- Usually needs fast and powerful hardware.
- It always needs validation of the results.
- Moreover, in most cases, it is not possible to accurately model all physical phenomena and a designer always needs simplistic assumptions.

LeFevre et al. [15] simulated the flow behavior in triangular cavities to predict solar still performance. They used different cover angles and proposed some correlations to estimate convective heat transfer coefficient in triangular solar stills. Chouikh et al. [16] analyzed the convective flow of combined buoyancy effects of mass and thermal diffusion in a sloped chamber. Ahmed et al. [17] presented a mathematical model for a solar water desalination system having multistepped distillation scheme to improve system productivity. They also used Fluent and Nastran software to simulate heat and mass transfer phenomena as well as structural analysis of the system. Xu et al. [18] studied and numerically analyzed a flat finned water desalination system using Fluent, where average and local heat transfer, velocity and temperature distributions were investigated. Results of Colburn and friction coefficient calculations illustrated that these values exhibit an increase by increasing Reynolds number. Rahman et al. [9,19] simulated double diffusive natural convection in two triangular enclosures, one of them had a corrugated bottom wall and the other had a flat bottom. They studied the effects of Rayleigh number and buoyancy ratio on the flow structure inside the cavities. Ching et al. [20] used the finite element method to simulate heat and mass transfer in a right triangular enclosure which is similar to single slope solar stills. They reported the direct effect of buoyancy ratio on heat and mass transfer inside the cavity. Ghachem et al. [21] used 3-D CFD simulation to investigate the flow structure inside a rectangular solar distiller. Rahbar and Esfahani [22,23] numerically simulated the flow patterns inside a single sloped solar still. They presented some models to obtain the approximate rate of pure water production and convective heat transfer coefficient. In another study, Rahbar et al. [24] simulated the flow structure inside a tubular solar still. They also provided some correlations to estimate convective heat transfer coefficient and water productivity inside the enclosure. Alvarado-Juárez et al. [25,26] used a 2-D finite volume method to solve governing equations of fluid flow inside an inclined cavity. They reported that $Ra_T = 10^6$, $A = 16$ and $\theta \geq 25°$ yielded the most suitable case for a solar still.

Weir-type cascade solar stills have caught much attention in recent years. In these systems, due to the lower space between glass and water, the empty space is rapidly saturated leading to higher efficiency as compared with that of other types of solar stills. Another advantage of such systems is their orientation adjustment capability for various latitudes, so that the maximum sunlight absorption can be guaranteed [27].

Velmurugan et al. [28] studied a 50 tray water desalination system with various heights. They also used sun absorbing materials (sponge, blade and gravel) to achieve higher solar absorption and an increased efficiency. Radhwan [29] evaluated the efficiency of a stepped water desalination system combined with a thermal energy storage reservoir. Dashtban and Tabrizi [30] and Tabrizi et al. [31] performed studies using thermal storage paraffin wax (phase change material [PCM]) beneath the absorbing plate. They reported that the system temperature was higher enough to produce distilled water in the absence of sunlight. This enhanced the system productivity by 31% as compared with that of a system without PCM. In other studies, Sarhaddi et al. [32], Tabrizi et al. [33] and Ziabari et al. [34] investigated the effects of using phase change materials on the performance and productivity of various stepped type solar stills. Omara et al. [35] used external and internal reflectors to enhance the productivity of a stepped solar still. El-Samadony et al. [36] used internal and external reflectors and an external condenser to enhance water productivity of a stepped solar still. They reported that the enhancement of productivity was about 66% and 165% higher than that of the conventional still for using reflectors and condenser, respectively.

Entropy can be defined as a measure of disorder within a thermodynamic system. Second law analysis shows that every irreversible system has an entropy generation greater than zero. This means that the system's irreversibilities reduce the useful work of the system [37–39]. For a solar still this useful work can be defined as pure water production inside the system. Heat transfer, fluid friction and mass transfer are the main reasons for existence of irreversibilities and entropy generation inside the solar stills. Lower entropy generation leads to higher useful work and higher water production inside a solar still. Therefore, many attentions have been made to study the entropy generation and exergy analysis in different configurations of solar stills [40–49].

Looking at the literature, most of the previous researches have been done on evaluation of overall entropy generation inside the solar stills. Generally, these studies are based on mathematical and experimental procedures. On the other hand, CFD methods provide the ability to obtain local entropy generation in a thermodynamic system [50]. In this way, it is possible to determine the exact location where the most entropy generation was happened. Hence, we have an opportunity to minimize the entropy generation and to improve the performance of the system by knowing these locations.

Number and height of steps can affect the flow pattern in a weir-type cascade solar still. It is clear that the change in flow pattern affects heat transfer, mass transfer and fluid friction, thus affecting the amount of entropy production within the enclosure. As mentioned before lower entropy production leads to higher water productivity inside the solar still. Therefore, it seems that there will be an optimal value for the number and dimension of steps. To the best knowledge of the authors of the present paper, there are not enough investigations on the effects of number and dimensions of steps on the performance of stepped type solar stills. Moreover, no research has been done on the effect of steps on the local

entropy production in the weir-type cascade solar stills. The aim of this study is to use the CFD to simulate the flow pattern and to estimate the local entropy generation inside a stepped type solar still. Moreover, optimum values for number of steps and their dimensions will be investigated.

2. Problem statement

2.1. Physical description

Fig. 1 shows a schematic view of the geometry used in this research. The model is a stepped type solar still with the length and height of 0.57 and 0.285 m, respectively. The system consists of a number of steps of length L and height d, a glass cover and two completely insulated vertical walls. Water and glass temperatures are assumed to be T_g and T_w, respectively. Investigating the effect of the number of steps on the still performance, 24 different models are considered. Table 1 summarizes characteristics of each of the models.

2.2. Mathematical formulation

In this study, the flow is assumed as 2-D, steady and laminar. In addition, uniform temperatures for water and glass and an adiabatic boundary condition for vertical walls were assumed. Moreover, the fluid has been considered as incompressible humid air with negligible viscous dissipation. Taking these assumptions, the governing equations including mass, momentum, energy and concentration conservation equations are as follows [5,51,52]:

$$\frac{\partial u}{\partial x} + \frac{\partial v}{\partial y} = 0 \tag{1}$$

$$u\frac{\partial u}{\partial x} + v\frac{\partial u}{\partial y} = -\frac{1}{\rho}\frac{\partial p}{\partial x} + \nu\left(\frac{\partial^2 u}{\partial x^2} + \frac{\partial^2 u}{\partial y^2}\right) \tag{2}$$

$$u\frac{\partial v}{\partial x} + v\frac{\partial v}{\partial y} = -\frac{1}{\rho}\frac{\partial p}{\partial y} + \nu\left(\frac{\partial^2 v}{\partial x^2} + \frac{\partial^2 v}{\partial y^2}\right) + \beta_T g\left(T - T_o\right) + \beta_s g\left(C - C_o\right) \tag{3}$$

$$u\frac{\partial T}{\partial x} + v\frac{\partial T}{\partial y} = \alpha\left(\frac{\partial^2 T}{\partial x^2} + \frac{\partial^2 T}{\partial y^2}\right) \tag{4}$$
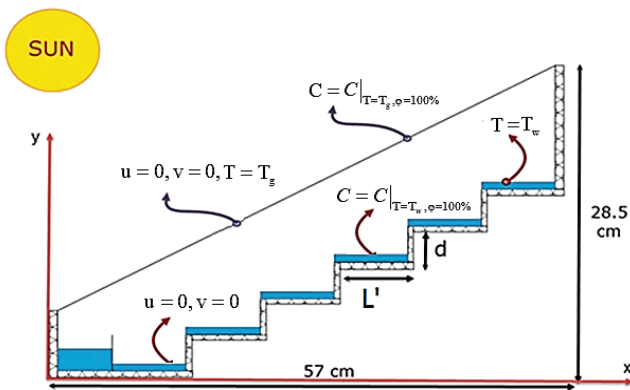

Fig. 1. Sketch of the geometry, boundary conditions and coordinate system of the solar still.

$$u\frac{\partial C}{\partial x} + v\frac{\partial C}{\partial y} = D_{AB}\left(\frac{\partial^2 C}{\partial x^2} + \frac{\partial^2 C}{\partial y^2}\right) \tag{5}$$

The boundary conditions are:

$$\text{On glass}: u = 0,\ v = 0,\ T = T_g,\ C = C\big|_{T=T_g,\ \varphi=100\%}$$

$$\text{On water}: u = 0,\ v = 0,\ T = T_w,\ C = C\big|_{T=T_w,\ \varphi=100\%} \tag{6}$$

$$\text{At both sides}: u = 0,\ v = 0,\ \frac{\partial T}{\partial x} = 0,\ \frac{\partial C}{\partial x} = 0$$

where

$$\beta_T = -\frac{1}{\rho_o}\left(\frac{\partial \rho_o}{\partial T}\right)_P,\quad \beta_s = -\frac{1}{\rho_o}\left(\frac{\partial \rho_o}{\partial C}\right)_P \tag{7}$$

In the above equations, saturated air properties such as specific heat, viscosity and thermal conductivity can be calculated according to the values given in Table 2.

For a 2-D flow, the local volumetric entropy generation, S_{gen}''', can be given as follows [53,54]:

$$S_{gen}''' = \frac{k}{T^2}\left[\left(\frac{\partial T}{\partial x}\right)^2 + \left(\frac{\partial T}{\partial y}\right)^2\right] + \frac{\mu}{T}\left[2\left(\left(\frac{\partial u}{\partial x}\right)^2 + \left(\frac{\partial v}{\partial y}\right)^2\right) + \left(\frac{\partial u}{\partial y} + \frac{\partial v}{\partial x}\right)^2\right]$$
$$+ \frac{RD_{AB}}{C}\left[\left(\frac{\partial C}{\partial x}\right)^2 + \left(\frac{\partial C}{\partial y}\right)^2\right] + \frac{RD_{AB}}{T}\left[\left(\frac{\partial C}{\partial x}\right)\left(\frac{\partial T}{\partial x}\right) + \left(\frac{\partial C}{\partial y}\right)\left(\frac{\partial T}{\partial y}\right)\right] \tag{8}$$

Table 1
Characteristics of various models used to simulate the problem

Case	No. of steps (n)	Length of steps L' (cm)	Height of steps d (cm)
1	4	12.5	2
2	4	12.5	3
3	4	12.5	4
4	4	12.5	5
5	5	10	2
6	5	10	3
7	5	10	3.5
8	5	10	4
9	5	10	4.5
10	6	8.33	2
11	6	8.33	2.5
12	6	8.33	3
13	6	8.33	3.5
14	6	8.33	4
15	7	7.14	2
16	7	7.14	2.5
17	7	7.14	3
18	7	7.14	3.5
19	8	6.25	2
20	8	6.25	2.5
21	8	6.25	3
22	9	5.55	2
23	10	5	2
24	12	4.16	2

Table 2
Properties of humid air at mean operating temperature [23]

Quantity	Expression
Specific heat	$C_p = 999.2 + 0.1434 \times T_i + 1.101 \times 10^{-4} \times T_i^2$ $- 6.758 \times 10^{-8} \times T_i^3$
Density	$\rho = 353.44/(T_i + 273.15)$
Thermal conductivity	$K = 0.0244 + 0.7673 \times 10^{-4} \times T_i$
Viscosity	$\mu = 1.718 \times 10^{-5} + 4.62 \times 10^{-8} \times T_i$
Mean temperature	$T_i = (T_g + T_w)/2$

The above equation indicates that local entropy generation in a heat and mass transfer process is due to heat transfer, fluid friction and mass transfer inside the flow field.

2.3. Solution procedures

A system of discretized equations was obtained by integrating the governing differential Eqs. (1)–(7) over an elementary control volume. More details about discretization procedure can be found in a paper by Rahbar and Esfahani [22]. SIMPLEC was used for pressure–velocity coupling, and line-by-line Thomas algorithms were employed to iteratively solve the prediscretized equations [55,56]. It was assumed that convergence is attained when the values of scaled residuals are smaller than a prescribed value of 10^{-3}, with an exception for the energy equation where this prescribed value is set at 10^{-6} [57,58].

Moreover, the following equations were used to calculate the average Nusselt number and the hourly yield (per unit area) of the stepped type solar still [23].

$$\text{Nu} = \frac{-H}{L(T_w - T_g)} \int_0^L \frac{\partial T}{\partial y}\bigg|_{\text{water}} dx \qquad (9)$$

$$\dot{m} = \frac{-3,600 \times D_{\text{AB}}}{L} \int_0^L \frac{\partial C}{\partial y}\bigg|_{\text{water}} dx \qquad (10)$$

Assessing the independence of solutions from grid size and eliminating errors resulted from grid roughness, numerical solutions for various grids of 1,300, 2,500, 5,000, 12,000 and 25,000 cells were also investigated. Fig. 2 represents the plot of grid independency test for the stepped type solar still. As can be seen, a grid of 12,000 elements was selected for solution process. The associated error with this grid differed less than 10% from that of a grid of 25,000 triangle elements. Maximum aspect ratio, minimum orthogonal quality and maximum ortho-skew quality were 4.46, 0.6 and 0.28, respectively. Moreover, to improve the solution accuracy, a finer grid was used near walls. Fig. 3 illustrates the implemented grid in this research.

To validate the CFD results, numerical solution of the present study has been evaluated by three methods. In the first method, a single slope solar still was simulated, solved and compared with the study of Rahbar and Esfahani [22]. Table 3 shows the comparison results revealing a maximum error of 8.4%.
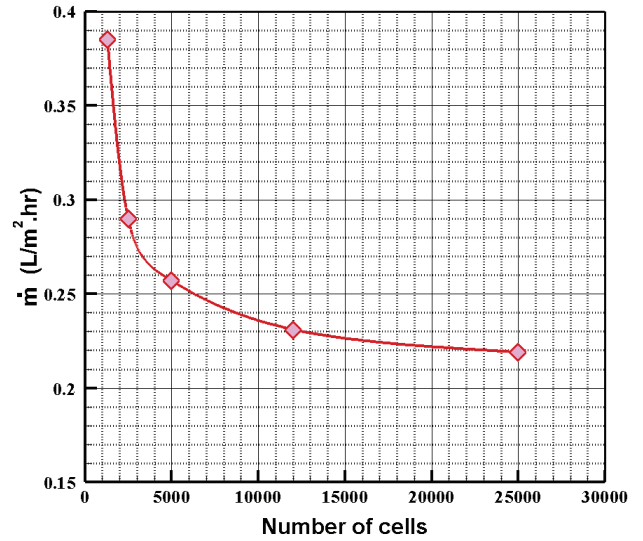

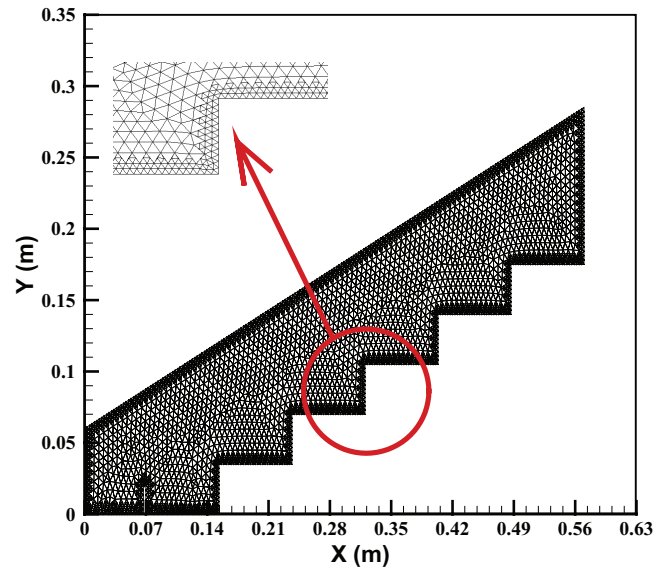Fig. 2. Grid dependency check for the solution.

Fig. 3. The implemented grid in numerical simulation of the weir-type cascade solar still.

Table 3
The comparison between the results of this study and Rahbar and Esfahani [22]

Case	T_w (K)	T_g (K)	Nu, Rahbar and Esfahani [22]	Nu, Present work	Error %
1	313	303	15.29	16.3	6.6
2	323	313	15.46	15.93	3
3	333	323	15.68	17	8.4
4	343	333	15.53	15.76	1.5

In the second method, double diffusive natural convection was simulated inside a simple square cavity and the results were compared with the study of Beghein et al. [59]. Table 4 shows different cases used in simulation of the cavity. Fig. 4 compares the results of CFD code with the results reported by Beghein et al. [59]. The maximum error between CFD and the results of Beghein et al. were 4.5% and 1.8% for local Nusselt number and local Sherwood number, respectively.

On the other hand, since the purpose of this work is to investigate the flow structure inside a stepped type solar still, experimental data from a real case have been compared with the results of numerical simulation. Data were obtained from an experiment performed in a summer day under the climatic conditions of Semnan (35°33′ N, 53°23′ E), Iran. The experiment was carried out from 10:00 to 14:00 and the solar still is positioned toward the south. When the air became saturated and the condensation on the glass was occurred, the glass temperature, water temperature and water productivity were measured. Figs. 5 and 6 show the setup used in the experiment, while Tables 5 and 6 provide the characteristics of the experimental facilities. More information about the calculation of the uncertainty of measuring devices (mentioned in Table 6) can be found in the literature [7,60].

Fig. 5. Photograph of the experimental setup at the beginning of the experiment.

Fig. 6. Experimental setup in the middle of the day.

Table 4
Different cases used in simulation of the square cavity

Case	1	2
Le	1	1
Pr	0.71	0.71
Ra_T	20,000	10,000
Br	0	1

Table 5
The geometry used in CFD simulation validation

The height of left side (solar still)	6 cm
The height of right side (solar still)	28.5 cm
Length of solar still	60 cm
Width of solar still	51 cm
No. of steps	10
Length of each step	5 cm
Height of each step	2 cm
Width of each step	50 cm

Table 6
Accuracies, ranges and standard uncertainty of measuring instruments

Instrument	Temperature sensor (type K) (°C)	Volume meter (mL)
Accuracy	0.1	0.2
Range	−100 to 1,300	0–5
Standard uncertainty	0.06	0.115

Fig. 4. Local Nusselt number on the left wall (for case 1, Table 4).

Table 7
A comparison between experimental data and numerical results

Case	1
Time	13:00–14:00
$\dot{m}$ From experiment (cc/m² h)	260
$\dot{m}$ From CFD simulation (cc/m² h)	231
Error %	11

As mentioned before, the air was assumed as saturated humid gas in the CFD simulation of the solar still. Thus, only the experimental data for saturated condition was chosen to compare with the CFD simulation. Note that, the saturated condition was occurred when continues condensation of water vapor took place on the glass cover (between 13 and 14 o'clock). Table 7 shows the comparison between CFD simulation and experimental procedure between 13 and 14 o'clock which has had 100% relative humidity of air. The result shows that the relative error for CFD simulation is about 11%, which is acceptable according to the following reasons:

- In real condition, front, rear and side walls have several effects on system efficiency, while in 2-D simulation, this fact is neglected.
- Under experimental condition, the glass has no uniform temperature on its various points. However, glass temperature is assumed to be uniform in numerical simulation.
- In real conditions, some water droplets remain on walls, while in numerical simulation, this fact is not taken into account.

3. Results and discussion

In this work, a stepped type solar still was numerically simulated. Since the purpose of this study has been to find the optimal geometry of the system, at first, the effect of number of steps on production rate of the system has been evaluated. Then, flow structure inside the system was simulated under various conditions.

Fig. 7 represents the effect of the number of steps on production rate where the glass and water temperatures were set to the values obtained at 14:00 when saturation conditions were well-established inside the solar still. As can be observed, taking a constant step height of 2 cm, the maximum water production rate is found to be 233 mL/m² h achieved with 7, 8 and 10 steps. It would be seen later that this is due to the structure of recirculating zones within the enclosure. As can be seen in Fig. 7, there is a sudden drop in water productivity for the value of nine steps. The reason for that is due to changing airflow pattern and structure. In fact, the geometry of a solar still can affect the flow structure inside the enclosure. This changes the flow strength and the time of vapor existence near the glass cover. This is the main reason for changing water productivity in different number of steps.

Step height affects the flow structure inside the enclosure, so as there will be an optimal value for step height.
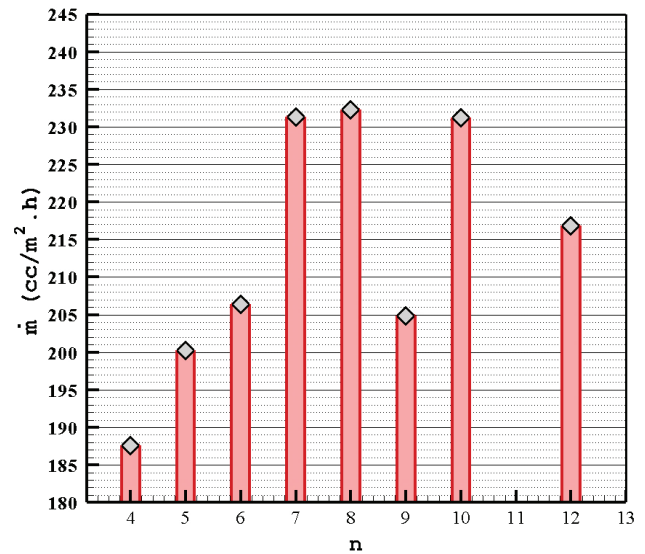

Fig. 7. Effect of the number of steps on productivity (d = 2 cm, T_w = 330 K and T_g = 318 K).

Fig. 8 represents the effects of step height on production rate of desalination systems with 4, 5, 6, 7 and 8 steps. As can be seen, the production rate is maximized by considering six steps of 3.5 cm height, while it is minimized when five steps of 3.5 cm height are considered. On the other hand, considering eight steps inside the solar still, there is more than 230 mL/m² h water productivity in all cases of steps height. It should be noted that, in solar still with seven steps of 2 cm height, production rate also increases considerably to reach an average amount of 231 ml/m² h.

Fig. 9 illustrates flow streamlines for various six-step solar stills. As it is mentioned before, the production rate is maximized by considering six steps of 3.5 cm height. This issue can be justified by referring to Fig. 9 wherein streamlines are depicted together with the number and regularity of recirculating zones. As the number of vortices increases, time for vapor approaching from water surface to glass will be shortened, so that an increase is expected within the distillation rate and system output. From Fig. 9, it is evident that in case (d), where step height is 3.5 cm, the number and regularity of vortices are more than other cases.

Figs. 10 and 11 represent temperature and concentration changes within desalination systems in various cases of six steps. The results showed that the variation of temperature for the most area of the solar still is about 2 K, while the variation of mass fraction was about 0.01. Moreover, temperature and concentration of the middle of recirculating zones has the values of 324 K and 0.09, respectively. This showed that the middle of recirculating zones has the average values of water and glass cover.

Fig. 12 illustrates variations of production rate as well as convective heat transfer between water and glass for various step heights in a six-step solar still. Obviously, increasing heat transfer rate, production rate increases as well. Higher Nusselt number will result in higher heat transfer rate within the system, which is due to more power of vortices. Indeed, heat
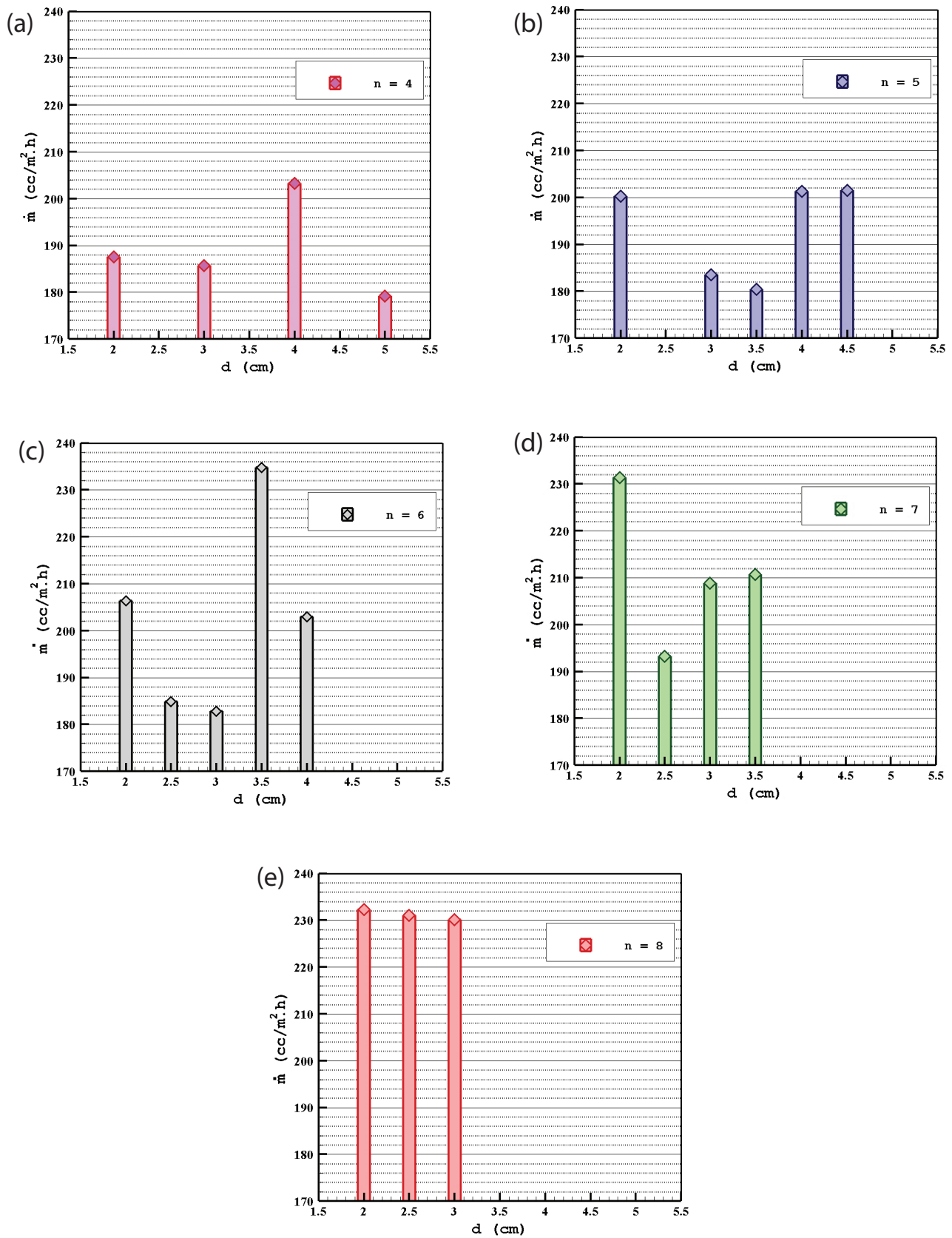
Fig. 8. The effect of height of steps on solar still productivity ($T_w = 330$ K and $T_g = 318$ K). (a) $n = 4$, (b) $n = 5$, (c) $n = 6$, (d) $n = 7$ and (e) $n = 8$.
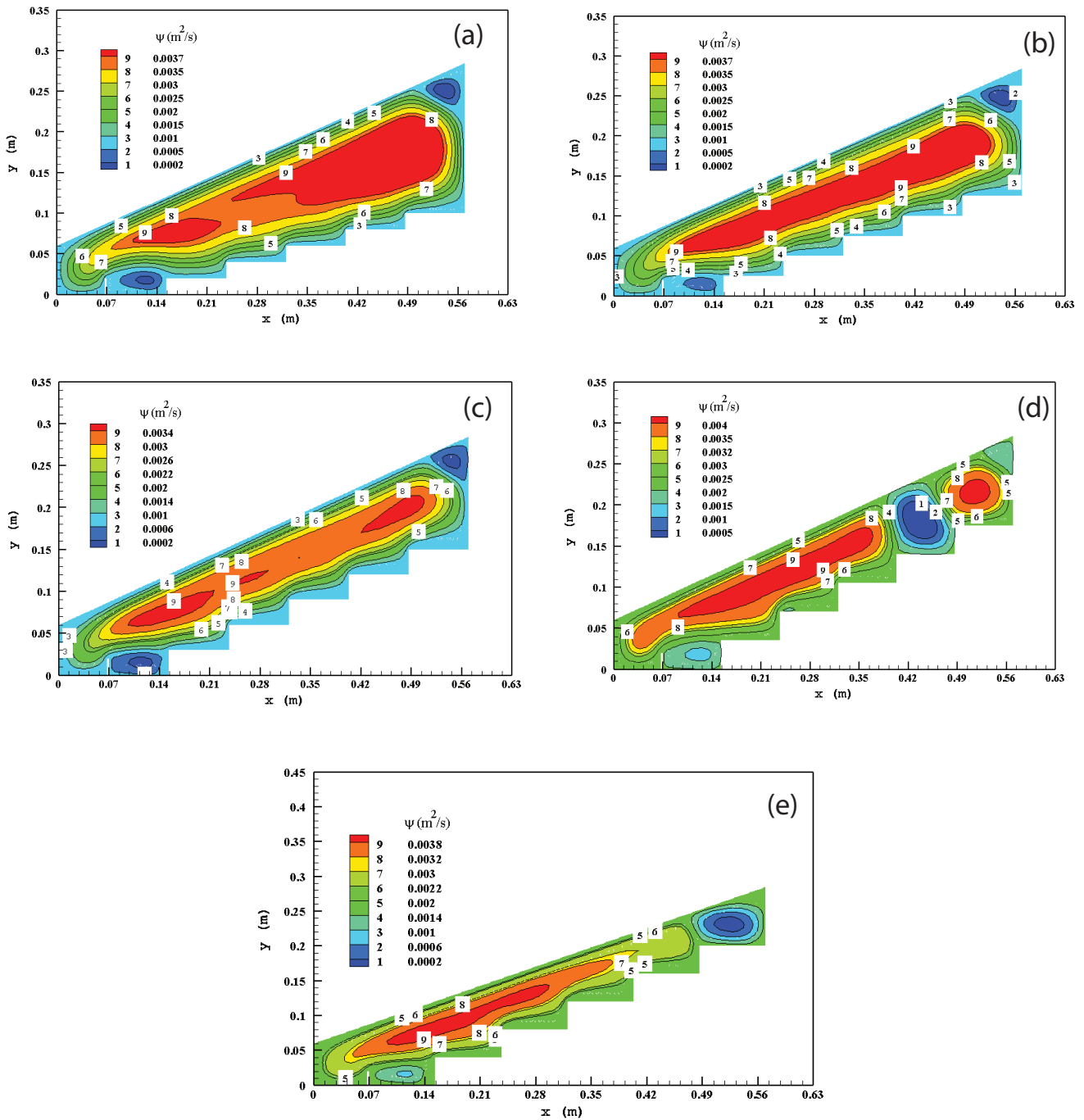
Fig. 9. Streamlines in solar still with six steps and various heights (T_w = 330 K and T_g = 318 K). (a) d = 2 cm, (b) d = 2.5 cm, (c) d = 3 cm, (d) d = 3.5 cm and (e) d = 4 cm.

transfer rate increases because vortices have enough time to absorb the heat. The important implication is that the changes in heat transfer rate are directly related to those in output of desalination system. This is in agreement with the findings of other researchers [24]. Maximum heat transfer rate and water productivity are about 18 W and 234 mL/m² h, respectively.

Fig. 13 shows local entropy generation inside the six steps solar stills with various step heights. The results showed that

the highest entropy production occurred at the edge of the stairs (due to the friction) and in the place of the rising and lowering of the recirculating zones (due to the temperature and concentration gradients). The results also indicated that the entropy generation is high along the water and glass, and it is low in the middle of the enclosure.

Fig. 14 shows contours of local entropy production near the vertical partition located at the bottom of the solar
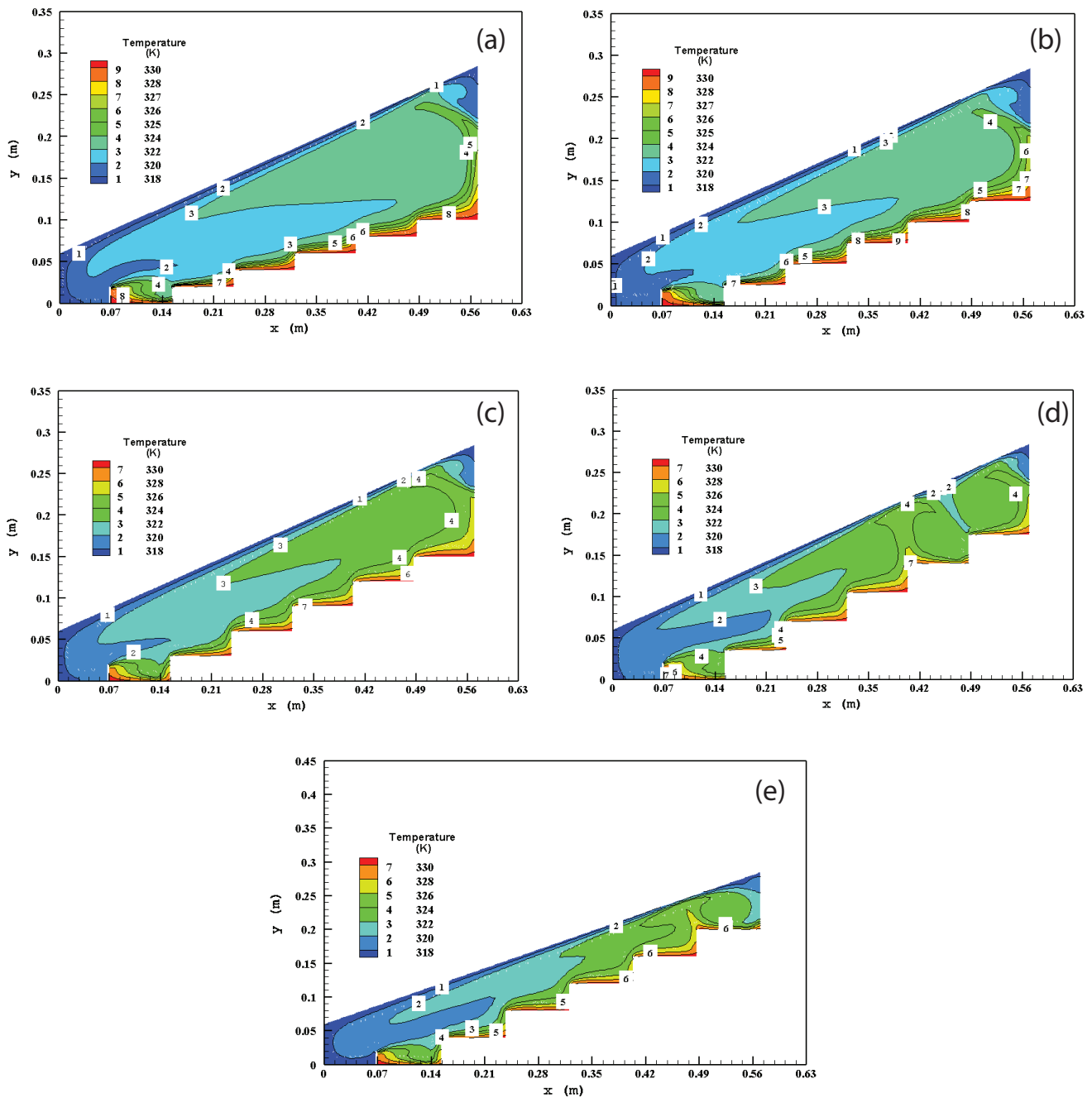
Fig. 10. Isotherms in solar still with six steps (T_w = 330 K and T_g = 318 K). (a) d = 2 cm, (b) d = 2.5 cm, (c) d = 3 cm, (d) d = 3.5 cm and (e) d = 4 cm.

still with 3.5 cm steps height (Fig. 13(d)). It is clear that due to the collision of air vortices with the partition, there is a high value of entropy production just after this area. On the other hand, there is a destructive vortex after the vertical partition which leads to a high amount of entropy production in this area. There is also a great amount of entropy production at the tip of the stairs. This is due to the friction between the fluid flow and the edge of the stairs.

Fig. 15 shows contours of local entropy production near the water surface and the glass cover for the solar still with 3.5 cm steps height (Fig. 13(d)). It is concluded that, there is a high amount of entropy production near the glass cover due to the heat transfer and condensation between humid air and the glass cover. On the other hand, there is also a high amount of entropy production near the water surface. This is due to the heat transfer and vaporization between the dry air vortices and the water surface.
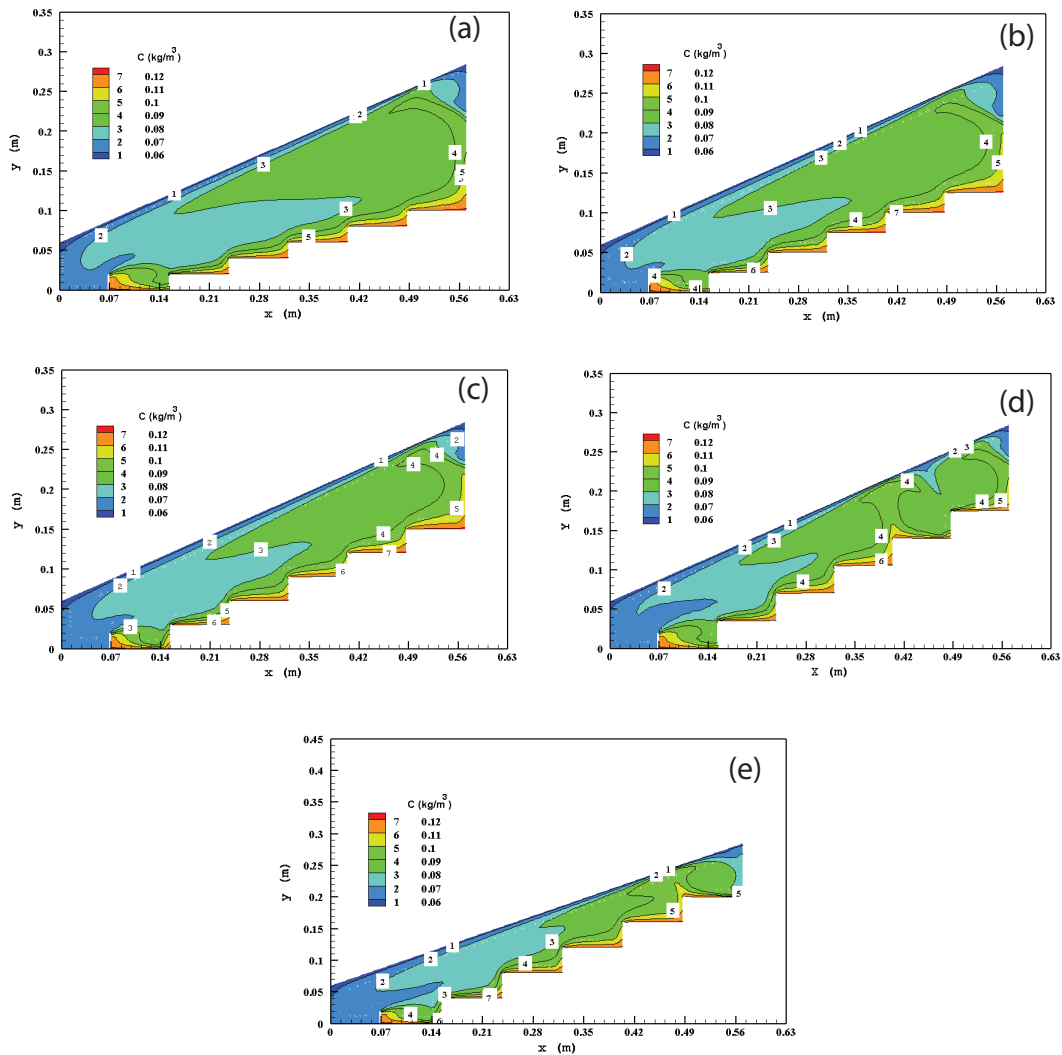
Fig. 11. Mass fraction in a solar still with six steps (T_w = 330 K and T_g = 318 K). (a) d = 2 cm, (b) d = 2.5 cm, (c) d = 3 cm, (d) d = 3.5 cm and (e) d = 4 cm.

4. Conclusions

In this paper, second law analysis and performance evaluation of weir-type cascade solar stills with different geometries have been studied using CFD simulation. The main conclusions can be summarized as follows:

- Considering a step height of 2 cm, having 7, 8 and 10 steps leads the system to achieve high water production. This is because of the regular structure of recirculating zones within the enclosure.
- Among different number of steps and various heights, the case of six steps of 3.5 cm height is the optimum geometry for the investigated solar still.
- Number of recirculating zones and their regularities are the main effective parameters on the productivity of the weir-type cascade solar still.
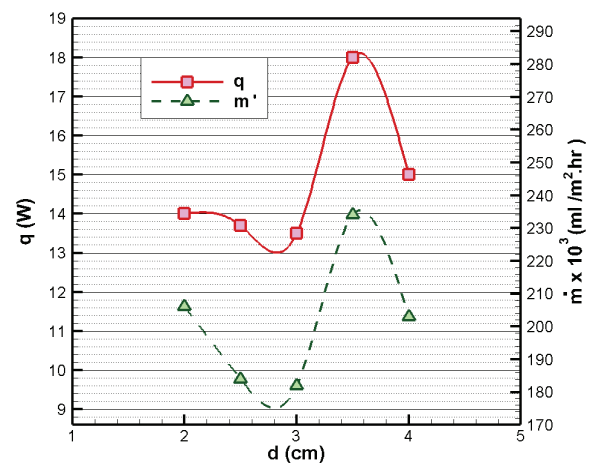- Increasing heat transfer rate between water and glass, the production rate increases as well.

Fig. 12. Heat transfer and water productivity for different step heights in a six-step solar still.
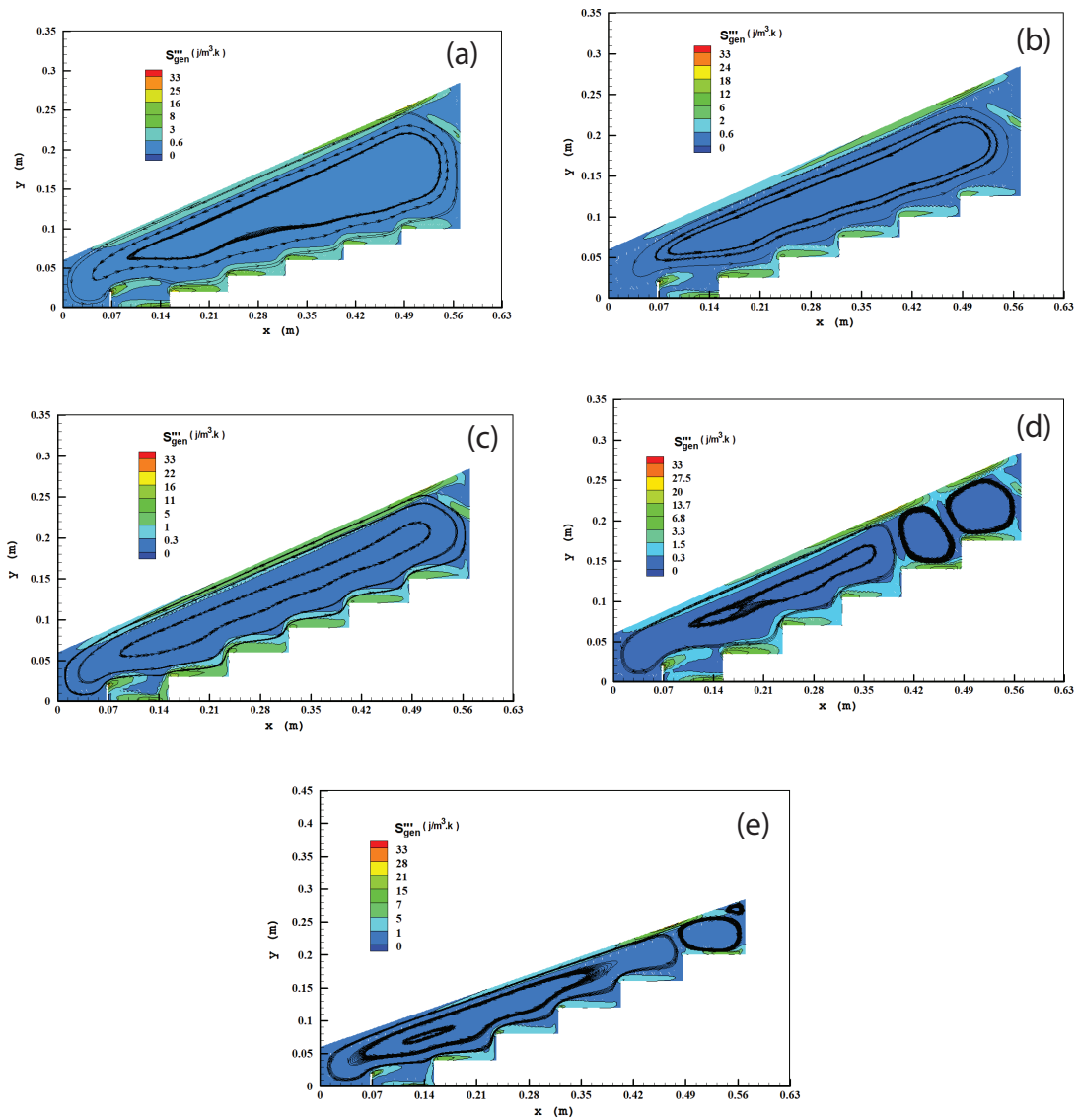
Fig. 13. Local entropy generation in solar still with six steps and various heights (T_w = 330 K and T_g = 318 K). (a) d = 2 cm, (b) d = 2.5 cm, (c) d = 3 cm, (d) d = 3.5 cm and (e) d = 4 cm.
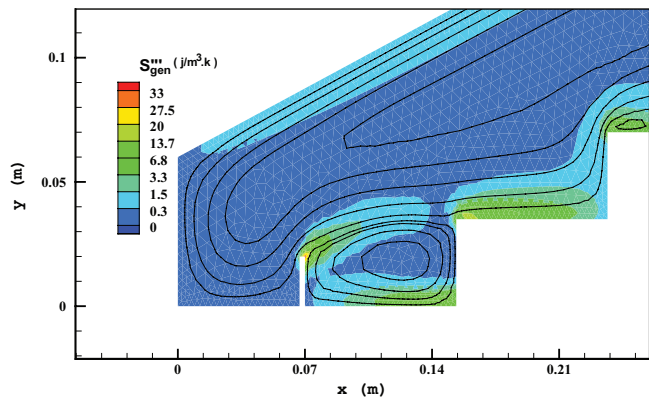

Fig. 14. Local entropy generation near the vertical partition in the bottom of solar still with six steps and d = 3.5 cm (T_w = 330 K and T_g = 318 K).
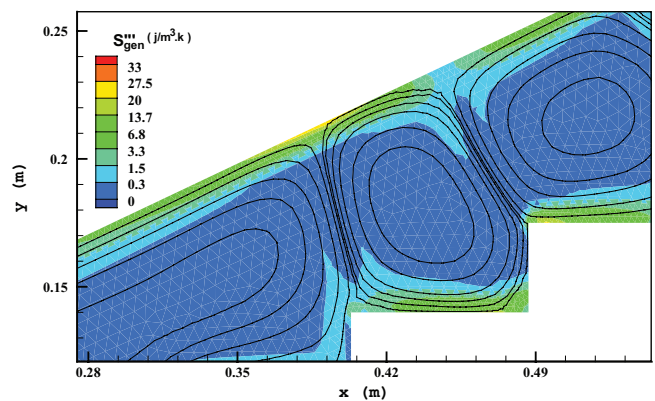
Fig. 15. Local entropy production near water and glass for the solar still with six steps and d = 3.5 cm (T_w = 330 K and T_g = 318 K).

- Maximum heat transfer rate and water productivity are about 18 W and 234 mL/m² h, respectively.
- Maximum entropy generation occurred at the edge of the stairs (due to the friction) and in the place of the rising and lowering of the recirculating zones (due to the temperature and concentration gradients).
- The entropy generation is high along the water and glass, and it is low in the middle of the enclosure.
- A destructive vortex exists after the vertical partition which leads to a high amount of entropy production.
- A great amount of entropy production was seen at the tip of the stairs which was due to the friction between the fluid flow and the edge of the stairs.
- There is also a high amount of entropy generation near the glass cover due to condensation and heat transfer between the humid air vortices and the glass.
- Moreover, a high amount of entropy production was seen near the water surface due to vaporization and heat transfer between the cold air and the water surface.

Acknowledgment

Symbols

A	—	Aspect ratio, L/h
Br	—	Buoyancy ratio, $\dfrac{\beta_s(c_w - c_g)}{\beta_T(T_w - T_g)}$
C_p	—	Specific heat, J/kg K
C	—	Vapor concentration of air, kg/m³
d	—	Height of steps, m
D_{AB}	—	Mass diffusivity of vapor, m/s
g	—	Gravitational acceleration, m/s²
H	—	Distance between water and glass, m
K	—	Thermal conductivity, W/m K
L	—	Length of solar still, m
L'	—	Length of steps, m
Le	—	Lewis number, $\alpha . D_{AB}^{-1}$
m''	—	Water productivity, kg/s m²
$\dot{m}$	—	Hourly water productivity, kg/h m²
n	—	Number of steps
Nu	—	Average Nusselt number
Nu_x	—	Local Nusselt number
p	—	Pressure, Pa
Pr	—	Prandtl number, $\nu\alpha^{-1}$
q	—	Convective heat transfer, W
R	—	Ideal gas constant, J/kg K
Ra_T	—	Thermal Rayleigh number, $g\beta_T H^3(T_w - T_g)(\nu\alpha)^{-1}$
x	—	X direction in Cartesian coordinate
y	—	Y direction in Cartesian coordinate
S'''_{gen}	—	Volumetric entropy generation, J/m³ K
T	—	Temperature, K
T_g	—	Glass temperature, K
T_i	—	Mean operating temperature, $0.5(T_w + T_g)$, °C
T_w	—	Water temperature, K
u	—	X-component of velocity, m/s
v	—	Y-component of velocity, m/s

Greek symbols

α	—	Thermal diffusivity of air, m²/s
β_T	—	Volume expansion coefficient, K⁻¹
β_s	—	Species expansion coefficient, kg/m³
φ	—	Relative humidity, %
μ	—	Dynamic viscosity, kg/m s
ν	—	Kinematic viscosity of air, m²/s
θ	—	Slope of glass
ρ	—	Density, kg/m³

Subscripts

w	—	Water
g	—	Glass
o	—	Operating condition
gen	—	Generation

References

[1] N. Rahbar, J.A. Esfahani, A. Asadi, An experimental investigation on productivity and performance of a new improved design portable asymmetrical solar still utilizing thermoelectric modules, Energy Convers. Manage., 118 (2016) 55–62.

[2] A. Heydari, N. Rahbar, Energy and life cost analysis of a wet wall solar still with various pump working conditions, Environ. Prog. Sustain., 36 (2017) 532–538.

[3] O. Mahian, A. Kianifar, S.Z. Heris, D. Wen, A.Z. Sahin, S. Wongwises, Nanofluids effects on the evaporation rate in a solar still equipped with a heat exchanger, Nano Energy, 36 (2017) 134–155.

[4] P. Refalo, R. Ghirlando, S. Abela, The effect of climatic parameters on the heat transfer mechanisms in a solar distillation still, Heat Transfer Eng., 35 (2014) 1473–1481.

[5] S. Rashidi, J. Abolfazli Esfahani, N. Rahbar, Partitioning of solar still for performance recovery: experimental and numerical investigations with cost analysis, Sol. Energy, 153 (2017) 41–50.

[6] N. Rahbar, A. Gharaiian, S. Rashidi, Exergy and economic analysis for a double slope solar still equipped by thermoelectric heating modules – an experimental investigation, Desalination, 420 (2017) 106–113.

[7] N. Rahbar, A. Asadi, Solar intensity measurement using a thermoelectric module; experimental study and mathematical modeling, Energy Convers. Manage., 129 (2016) 344–353.

[8] S. Rashidi, M. Bovand, N. Rahbar, J.A. Esfahani, Steps optimization and productivity enhancement in a nanofluid cascade solar still, Renew. Energy, 118 (2018) 536–545.

[9] M.M. Rahman, H.F. Öztop, A. Ahsan, M.A. Kalam, Y. Varol, Double-diffusive natural convection in a triangular solar collector, Int. Commun. Heat Mass Transfer, 39 (2012) 264–269.

[10] A. Heydari, M. Shateri, S. Sanjari, Numerical analysis of a small size baffled shell-and-tube heat exchanger using different nano-fluids, Heat Transfer Eng., 39 (2018) 141–153.

[11] R. Sabbagh, N. Rahbar, Numerical study on the effect of geometrical parameters on flare tip wall temperature and emission, J. Model. Eng., 13 (2015) 43–57.

[12] N. Rahbar, M. Shateri, M. Taherian, M.S. Valipour, 2D numerical simulation of a micro scale Ranque-Hilsch vortex tube, J. Heat Mass Transfer Res., 2 (2015) 39–48.

[13] N. Rahbar, M. Taherian, M. Shateri, S.M. Valipour, Numerical investigation on flow behavior and energy separation in a micro-scale vortex tube, Therm. Sci., 19 (2015) 619–630.

[14] S. Rashidi, N. Rahbar, M. Sadegh Valipour, J. Abolfazli Esfahani, Enhancement of solar still by reticular porous media: experimental investigation with exergy and economic

analysis, Appl. Therm. Eng., 130 (2018) 1341–1348. https://doi.org/10.1016/j.applthermaleng.2017.11.089.

[15] J. LeFevre, W.J. Bowman, M.R. Jones, Numerical simulation of convection in triangular cavities to predict solar still performance, J. Thermophys. Heat Transfer, 27 (2013) 482–488.

[16] R. Chouikh, L. Ben Snoussi, A. Guizani, Numerical study of the heat and mass transfer in inclined glazing cavity: application to a solar distillation cell, Renew. Energy, 32 (2007) 1511–1524.

[17] M.I. Ahmed, M. Hrairi, A.F. Ismail, On the characteristics of multistage evacuated solar distillation, Renew. Energy, 34 (2009) 1471–1478.

[18] S. Xu, X. Ling, H. Peng, Simulation of heating cell in a new integrated solar plate-fin desalination unit by fluent, Inf. Technol. J., 10 (2011) 2446–2451.

[19] M.M. Rahman, R. Saidur, S. Mekhilef, M.B. Uddin, A. Ahsan, Double-diffusive buoyancy induced flow in a triangular cavity with corrugated bottom wall: effects of geometrical parameters, Int. Commun. Heat Mass Transfer, 45 (2013) 64-74.

[20] Y.C. Ching, H.F. Öztop, M.M. Rahman, M.R. Islam, A. Ahsan, Finite element simulation of mixed convection heat and mass transfer in a right triangular enclosure, Int. Commun. Heat Mass Transfer, 39 (2012) 689–696.

[21] K. Ghachem, L. Kolsi, C. Mâatki, A.K. Hussein, M.N. Borjini, Numerical simulation of three-dimensional double diffusive free convection flow and irreversibility studies in a solar distiller, Int. Commun. Heat Mass Transfer, 39 (2012) 869–876.

[22] N. Rahbar, J.A. Esfahani, Productivity estimation of a single-slope solar still: theoretical and numerical analysis, Energy, 49 (2013) 289–297.

[23] N. Rahbar, J.A. Esfahani, Estimation of convective heat transfer coefficient in a single-slope solar still: a numerical study, Desal. Wat. Treat., 50 (2012) 387–396.

[24] N. Rahbar, J. Abolfazli Esfahani, E. Fotouhi-Bafghi, Estimation of convective heat transfer coefficient and water-productivity in a tubular solar still – CFD simulation and theoretical analysis, Sol. Energy, 113 (2015) 313–323.

[25] R. Alvarado-Juárez, G. Álvarez, J. Xamán, I. Hernández-López, Numerical study of conjugate heat and mass transfer in a solar still device, Desalination, 325 (2013) 84–94.

[26] R. Alvarado-Juárez, J. Xamán, G. Álvarez, I. Hernández-López, Numerical study of heat and mass transfer in a solar still device: effect of the glass cover, Desalination, 359 (2015) 200–211.

[27] S.A. El-Agouz, Experimental investigation of stepped solar still with continuous water circulation, Energy Convers. Manage., 86 (2014) 186–193.

[28] V. Velmurugan, K.N. Kumar, T.N. Haq, K. Srithar, Performance analysis in stepped solar still for effluent desalination, Energy, 34 (2009) 1179–1186.

[29] A.M. Radhwan, Transient performance of a stepped solar still with built-in latent heat thermal energy storage, Desalination, 171 (2005) 61–76.

[30] M. Dashtban, F.F. Tabrizi, Thermal analysis of a weir-type cascade solar still integrated with PCM storage, Desalination, 279 (2011) 415–422.

[31] F.F. Tabrizi, M. Dashtban, H. Moghaddam, Experimental investigation of a weir-type cascade solar still with built-in latent heat thermal energy storage system, Desalination, 260 (2010) 248–253.

[32] F. Sarhaddi, F.F. Tabrizi, H.A. Zoori, S.A.H.S. Mousavi, Comparative study of two weir type cascade solar stills with and without PCM storage using energy and exergy analysis, Energy Convers. Manage., 133 (2017) 97–109.

[33] F.F. Tabrizi, M. Dashtban, H. Moghaddam, K. Razzaghi, Effect of water flow rate on internal heat and mass transfer and daily productivity of a weir-type cascade solar still, Desalination, 260 (2010) 239–247.

[34] F.B. Ziabari, A.Z. Sharak, H. Moghadam, F.F. Tabrizi, Theoretical and experimental study of cascade solar stills, Sol. Energy, 90 (2013) 205–211.

[35] Z.M. Omara, A.E. Kabeel, M.M. Younes, Enhancing the stepped solar still performance using internal and external reflectors, Energy Convers. Manage., 78 (2014) 876–881.

[36] Y. El-Samadony, A. Abdullah, Z. Omara, Experimental study of stepped solar still integrated with reflectors and external condenser, Exp. Heat Transfer, 28 (2015) 392–404.

[37] Y.A. Cengel, M.A. Boles, Thermodynamics: an engineering approach, Sea, 1000 (2002) 8862.

[38] M.J. Moran, H.N. Shapiro, D.D. Boettner, M.B. Bailey, Fundamentals of Engineering Thermodynamics, John Wiley & Sons, West Sussex, England, 2010.

[39] R.E. Sonntag, C. Borgnakke, G.J. Van Wylen, S. Van Wyk, Fundamentals of Thermodynamics, Wiley, New York, 2003.

[40] M. Asbik, O. Ansari, A. Bah, N. Zari, A. Mimet, H. El-Ghetany, Exergy analysis of solar desalination still combined with heat storage system using phase change material (PCM), Desalination, 381 (2016) 26–37.

[41] X. Wang, Y. Tang, Exergetic analysis on the two-stage reverse osmosis seawater desalination system, Desal. Wat. Treat., 51 (2013) 2862–2870.

[42] A. Sethi, V. Dwivedi, Exergy analysis of double slope active solar still under forced circulation mode, Desal. Wat. Treat., 51 (2013) 7394–7400.

[43] K.R. Ranjan, S.C. Kaushik, Energy, exergy and thermo-economic analysis of solar distillation systems: a review, Renew. Sustain. Energy Rev., 27 (2013) 709–723.

[44] V. Manikandan, K. Shanmugasundaram, S. Shanmugan, B. Janarthanan, J. Chandrasekaran, Energy, exergy and entropy analysis of a single-slope floating-cum-tilted wick-type solar still, Int. J. Ambient Energy, 53 (2013) 2–12.

[45] S. Kaushik, K. Ranjan, N. Panwar, Optimum exergy efficiency of single-effect ideal passive solar stills, Energy Effic., 6 (2013) 595–606.

[46] H. Aghaei Zoori, F. Farshchi Tabrizi, F. Sarhaddi, F. Heshmatnezhad, Comparison between energy and exergy efficiencies in a weir type cascade solar still, Desalination, 325 (2013) 113–121.

[47] A. Kianifar, S. Zeinali Heris, O. Mahian, Exergy and economic analysis of a pyramid-shaped solar water purification system: active and passive cases, Energy, 38 (2012) 31–36.

[48] V.G. Gude, N. Nirmalakhandan, S. Deng, A. Maganti, Desalination at low temperatures: an exergy analysis, Desal. Wat. Treat., 40 (2012) 272–281.

[49] G. Tiwari, V. Dimri, A. Chel, Exergetic analysis of passive and active solar stills, Int. J. Exergy, 5 (2008) 360–373.

[50] A. Bejan, Entropy Generation Through Heat and Fluid Flow, Wiley, New York, 1982.

[51] W.M. Kays, M.E. Crawford, B. Weigand, Convective Heat and Mass Transfer, 4th ed., McGraw-Hill, Singapore, 2005.

[52] P. Talukdar, C.R. Iskra, C.J. Simonson, Combined heat and mass transfer for laminar flow of moist air in a 3D rectangular duct: CFD simulation and validation with experimental data, Int. J. Heat Fluid Flow, 51 (2008) 3091–3102.

[53] H.F. Oztop, K. Al-Salem, A review on entropy generation in natural and mixed convection heat transfer for energy systems, Renew. Sustain. Energy Rev., 16 (2012) 911–920.

[54] A. Bejan, The thermodynamic design of heat and mass transfer processes and devices, Int. J. Heat Fluid Flow, 8 (1987) 258–276.

[55] S.V. Patankar, Numerical Heat Transfer and Fluid Flow, Hemisphere Publishing Corporation, USA, 1980.

[56] H.K. Versteeg, W. Malalasekera, An Introduction to Computational Fluid Dynamics: The Finite Volume Method, Prentice Hall, New York, 2007.

[57] A. Omri, Numerical investigation on optimization of a solar distiller dimensions, Desalination, 206 (2007) 373–379.

[58] M.M. Rahman, H.F. Öztop, A. Ahsan, J. Orfi, Natural convection effects on heat and mass transfer in a curvilinear triangular cavity, Int. J. Heat Mass Transfer, 55 (2012) 6250–6259.

[59] C. Beghein, F. Haghighat, F. Allard, Numerical study of double-diffusive natural convection in a square cavity, Int. J. Heat Mass Transfer, 35 (1992) 833–846.

[60] M. Hasani, N. Rahbar, Application of thermoelectric cooler as a power generator in waste heat recovery from a PEM fuel cell – an experimental study, Int. J. Hydrogen Energy, 40 (2015) 15040–15051.